

Highly efficient nickel-niobia composite catalysts for hydrogenation of CO₂ to methane

Edwin S. Gnanakumar^a, Narendraraj Chandran^b, Ivan V. Kozhevnikov^c, Aida Grau-Atienza^d, Enrique V. Ramos Fernández^d, Antonio Sepulveda-Escribano^d, N. Raveendran Shiju^{a,*}

^a Van't Hoff Institute for Molecular Sciences, University of Amsterdam, P.O. Box 94157, 1090GD Amsterdam, The Netherlands

^b Centre for Nano Science & Engineering, Indian Institute of Science, Bangalore, India

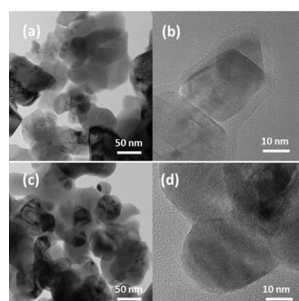
^c Department of Chemistry, University of Liverpool, Liverpool L69 7ZD, UK

^d Departamento de Química Inorgánica-Instituto Universitario de Materiales de Alicante, Laboratorio de Materiales Avanzados, Universidad de Alicante, Apartado 99, 03080 Alicante, Spain

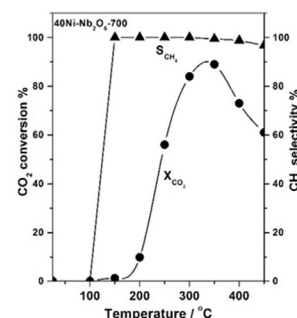
HIGHLIGHTS

- Heterogeneous catalysts based on nickel supported on niobia are synthesised.
- The catalysts are tested in CO₂ hydrogenation to methane in a packed bed reactor.
- The catalysts are active and highly selective in CO₂ methanation.
- A continuous test of 50 h confirmed the stability of the catalysts.
- The catalytic performance depends on the treatment temperature and niobia loading.

GRAPHICAL ABSTRACT



Ni-Nb₂O₅ catalysts give high activity and selectivity in CO₂ methanation



ARTICLE INFO

Article history:

Received 31 March 2018

Received in revised form 5 August 2018

Accepted 18 August 2018

Available online 19 August 2018

Keywords:

Niobia
CO₂ utilisation
Methanation
Nickel
Heterogeneous catalysis
Methane

ABSTRACT

We studied the catalytic hydrogenation of CO₂ to methane using nickel-niobia composite catalysts. Catalysts containing 10–70 wt% Ni were synthesized by wet impregnation and tested for CO₂ hydrogenation in a flow reactor. 40 wt% was found to be the optimum Ni loading, which resulted in CO₂ conversion of 81% at 325 °C. We also calcined the Nb₂O₅ support at different temperatures to study the influence of calcination temperature on the catalytic performance. 40 wt% Ni loaded on Nb₂O₅, which was calcined at 700 °C gave higher methanation activity (91% conversion of CO₂). Time on stream study for 50 h showed a stable activity and selectivity; thus confirming the scope for practical application.

© 2018 Published by Elsevier Ltd.

1. Introduction

Increase in the concentration of CO₂ on earth atmosphere can cause various effects in the climate and is becoming a major threat

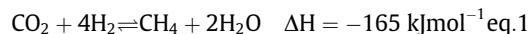
* Corresponding author.

E-mail address: n.r.shiju@uva.nl (N.R. Shiju).

to the living beings (Crowley, 2000; Meehl et al., 2005). Therefore, significant efforts are being invested to deal with CO₂ emission and its consequences (Davis et al., 2010; Friedlingstein et al., 2010; Yang et al., 2008; Yu et al., 2008; Saeidi et al., 2014). Recently, in Paris, the United Nations conference on climatic change emphasized the importance of controlling the greenhouse gas emissions, particularly CO₂ (Rockström et al., 2017). Simultaneous efforts are

needed to decrease the CO₂ emission and for the active removal of CO₂ accumulated on earth atmosphere. Converting CO₂ into commercial chemicals and fuels is one of the practical ways for CO₂ mitigation (Saeidi et al., 2014; Daza and Kuhn, 2016; Porosoff et al., 2016). CO₂ hydrogenation to methane (synthetic natural gas/SNG) is one of the ways to do this (see equation 1 below). Methane is a promising hydrogen carrier due to the well-established liquefaction of natural gas and its safe transportation (Tada et al., 2012). Also this method integrates renewable resources (wind and solar energy) into the current energy mix efficiently. This is widely used in the power to gas concept (P2G) (Götz et al., 2016; Zhang et al., 2017), which was introduced for the conversion of renewable electrical power into a gaseous energy carrier such as methane. Since the surplus renewable power can be converted to gases, P2G will be important in the future energy system. The gases can be then used for transportation, domestic heating, feedstock and in power generation. While P2G may not be feasible and economical at all geographical locations, it is promising in Europe due to the increasing share of renewable electricity. P2G is a potential option to match the demand and supply of renewable power generation as the solar and wind-based power fluctuates. The existing gas infrastructure in Europe can accommodate large amounts of gas produced using this technology. Several European electrical companies have formed a consortium to implement the P2G concept. Thus, P2G has a promising future in European situation.

Methanation of CO₂ further finds application in the process of ammonia production to purify the feed (Khorsand et al., 2007). Interestingly, methanation of CO₂ has been proposed to reduce the cost of manned exploration of Mars. In this proposal, H₂ will be transported to Mars from earth and will be reacted with atmospheric CO₂ to form methane and water. Methane can be stored as fuel and water will be electrolyzed to oxygen for life support. H₂ will be recycled for the methanation with CO₂ (Junaedi et al., 2011; Wei and Jinlong, 2011). Moreover, its thermodynamic advantage makes methanation of CO₂ one of the promising processes for converting CO₂ into fuels (Aziz et al., 2015; Gao et al., 2012). This reaction is considerably faster than reactions to produce alcohols and other hydrocarbons (Aziz et al., 2015; Inui and Takeguchi, 1991). Thus, methanation of CO₂ gained more attention recently.



CO₂ hydrogenation was studied previously using a number of heterogeneous catalysts such as Rh, Ru, Pd, Ni, Co and mixed metals supported on metal oxides such as TiO₂, Al₂O₃, CeO₂ and ZrO₂ (Aziz et al., 2015; Frontera et al., 2017; Polanski et al., 2017; Wang et al., 2011). Among these metals, Ni based catalysts were investigated largely because of its abundance and low cost. They usually require more than 350 °C for high activity. However, at high temperatures, these catalysts deactivate rapidly due to Ni agglomeration, formation of volatile Ni(CO)₄ and coke deposition (Lu et al., 2014; Cai et al., 2013; Wachs, 2005; Zhou et al., 2015; Nie et al., 2017; Bajpai et al., 1982; Barrientos et al., 2014). Sometimes, selectivity towards methane is low due to the formation of by-products, particularly CO. Nature of the support plays an important role in supported metal catalysts, as the interaction between metal and support determines the activity and selectivity (Mejia et al., 2016; Batyrev et al., 2012). In general, high surface area supports are preferred for such reactions. Here, we use niobium pentoxide (niobia) as a support for nickel for CO₂ methanation reaction.

Niobium pentoxide is known for catalyzing several acid catalyzed reactions because of its acidity and stability in water as well as for catalyzing redox and photocatalytic reactions (Nair et al., 2012; Nowak and Ziolk, 1999; Shiju et al., 2010). Niobia

supported catalysts are widely studied for Fischer-Tropsch synthesis (den Otter et al., 2014; Frydman et al., 1999; den Otter et al., 2016), oxidation reactions (Jardim et al., 2015; Mozer and Passos, 2011; Rojas et al., 2009), and hydrodechlorination (Chary et al., 2004). A strong metal support interaction (SMSI) is observed for metals supported on niobia (Wojcieszak et al., 2006). This interaction could generate more active and selective sites, thus facilitating the reactions in the desired route. Hence, in our current work, we have chosen Nb₂O₅ as a support for CO₂ hydrogenation reaction. According to our knowledge, there is no previous report on CO₂ hydrogenation to methane using Nb₂O₅ as a support.

We impregnated the niobia support with different amounts of Ni and screened them for methanation reaction. Among those, 40 wt% Ni loaded on Nb₂O₅ pre-treated at 700 °C showed maximum CO₂ conversion of 91% and >99% selectivity towards methane at 350 °C. The results suggest that the amount of nickel and calcination temperature of the support play important roles in the performance of catalysts. Time on stream (TOS) study shows that the same catalyst is stable and active up to 50 h without any deactivation. Spent catalyst characterization shows the presence of metallic nickel particles, which did not change in size significantly under reaction conditions.

2. Materials and methods

2.1. Materials

All chemicals used in this work were used as received. Niobic acid was obtained from CBMM and Ni(NO₃)₂·6H₂O was purchased from Alfa Aesar. Deionised water was used for all impregnation experiments.

2.2. Synthesis of catalysts

Nickel-niobia composite catalysts were synthesized by wet impregnation method. Before impregnation, niobic acid was calcined at 500 °C for 4 h to obtain Nb₂O₅. Ni(NO₃)₂·6H₂O was used as the precursor for nickel. The synthesis procedure of 10 wt% Ni on Nb₂O₅ is given as an example: 1.98 g of Ni(NO₃)₂·6H₂O was dissolved in 30 ml of water in a 200 ml round bottom flask. Then 3.6 g of Nb₂O₅ was added to the above solution. The whole mixture was kept stirring at 75 °C for 24 h. The obtained powder was further dried at 150 °C for 12 h. Finally, the powder was calcined at 400 °C to get 10 wt% Ni-Nb₂O₅ catalyst. Similarly, other loadings such as 20, 30, 40, 50 and 70 wt% Ni-Nb₂O₅ catalysts were synthesized. To study the effect of pre-treatment, we also calcined niobic acid at 700 °C and 900 °C before loading nickel. Final calcination of all catalysts was done at 400 °C. The catalysts are labelled as follows: nNi-Nb₂O₅-T (n is wt% of nickel and T is the pre-treatment temperature of Nb₂O₅). For comparison, we also used niobic acid as such as a support for 40 wt% Ni loading.

2.3. Instrumentation

X-ray diffraction patterns of the samples were recorded using Rigaku Miniflex II diffractometer using Ni-filtered Cu K α ($\lambda = 1.5406 \text{ \AA}$) radiation. The X-ray tube was operated at 30 kV and 15 mA. Measurements were recorded in the 2 θ range from 10° to 80° with an angular step size of 0.05° and a counting time of 5° min⁻¹. Average crystallite size was calculated using Scherrer equation from the full width at half maximum (FWHM) of most intense XRD peak. Surface areas of the samples were determined by BET method using N₂ as adsorbent with multipoint modes at -196 °C. DRIFT (Diffuse Reflectance Infrared Fourier Transform) spectra of adsorbed pyridine were recorded on a Nicolet Nexus

FTIR spectrometer using powdered 1:4 w/w catalyst mixtures with KBr. The catalyst-KBr mixtures were pre-treated at $150\text{ }^{\circ}\text{C}/3 \times 10^{-3}\text{ mmHg}$ for 2 h, then exposed to pyridine vapour at room temperature for 1 h, followed by pumping out at $150\text{ }^{\circ}\text{C}/3 \times 10^{-3}\text{ mmHg}$ for 1 h to remove physisorbed pyridine. The DRIFT spectra of adsorbed pyridine were recorded at room temperature at a 4 cm^{-1} resolution against 1:4 w/w catalyst-KBr mixture treated at $150\text{ }^{\circ}\text{C}/3 \times 10^{-3}\text{ mmHg}$ for 2 h. XPS spectra were collected using a Thermo Scientific K-ALPHA with Al-K radiation (1486.6 eV), monochromatized by a twin crystal monochromator, yielding a focused X-ray spot with a diameter of $400\text{ }\mu\text{m}$, at $3\text{ mA} \times 12\text{ kV}$ when charge compensation was achieved with the system flood gun that provides low energy electrons and low energy argon ions from a single source. The alpha hemispherical analyzer was operated in the constant energy mode with survey scan pass energies of 200 eV to measure the whole energy band and with 50 eV in a narrow scan to selectively measure the particular elements. An estimation of the intensities was done after a calculation of each peak integral, S-shaped background subtraction and fitting the experimental curve to a combination of a Lorentzian (30%) and

Gaussian (70%) lines. Binding energies (BE), referenced to the C 1s line at 284.6 eV , have an accuracy of $\pm 0.1\text{ eV}$. Temperature-programmed desorption of ammonia ($\text{NH}_3\text{-TPD}$) measurements were carried out in a U-shaped quartz reactor. An amount of 100 mg of each catalyst was first pre-heated at $200\text{ }^{\circ}\text{C}$ with a He flow of $50\text{ cm}^3\text{ min}^{-1}$ for 1.5 h to remove the physisorbed molecules. The sample was exposed to NH_3 gas flow of $50\text{ cm}^3\text{ min}^{-1}$ for 10 min at room temperature. Subsequently, the system was heated to $850\text{ }^{\circ}\text{C}$ with a heating rate of $10\text{ }^{\circ}\text{C min}^{-1}$. The desorbed NH_3 was monitored by mass spectrometry. Transmission electron microscopy (TEM) images have been recorded using FEI-Thermo Fisher Scientific-Titan Themis 80–300 kV FEG electron microscope operating at 300 kV . Samples were uniformly dispersed in isopropanol before depositing on carbon holey grid.

2.4. Catalytic activity test

Hydrogenation of CO_2 was carried out using a fixed bed catalytic reactor equipped with stainless steel tube reactor. The gas flows were controlled using mass flow controllers. 1 g of catalyst

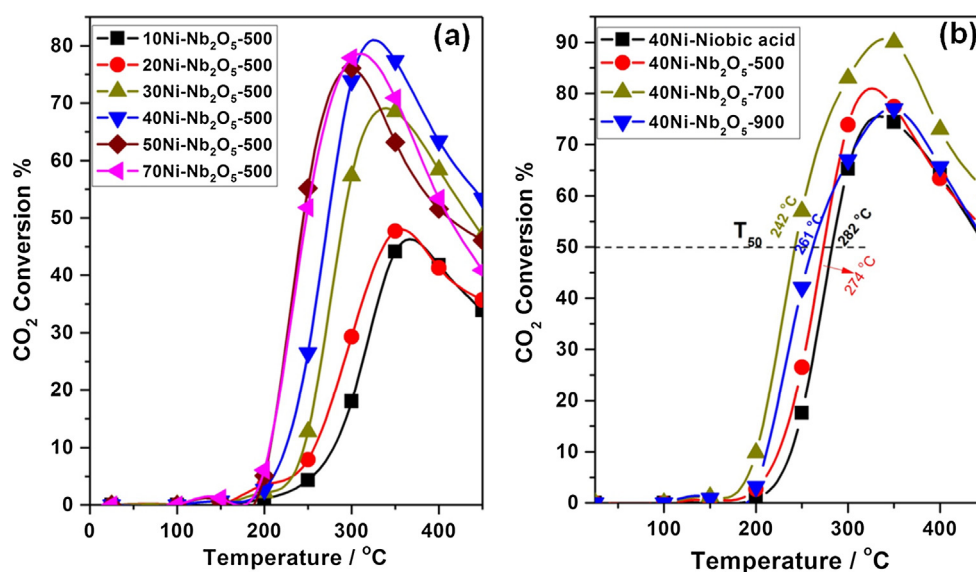


Fig. 1. (a) CO_2 methanation results for Ni/ Nb_2O_5 catalysts with different Ni loading and (b) $40\text{Ni-Nb}_2\text{O}_5\text{-T}$ catalysts in fixed bed reactor with GHSV of $750/\text{h}$.

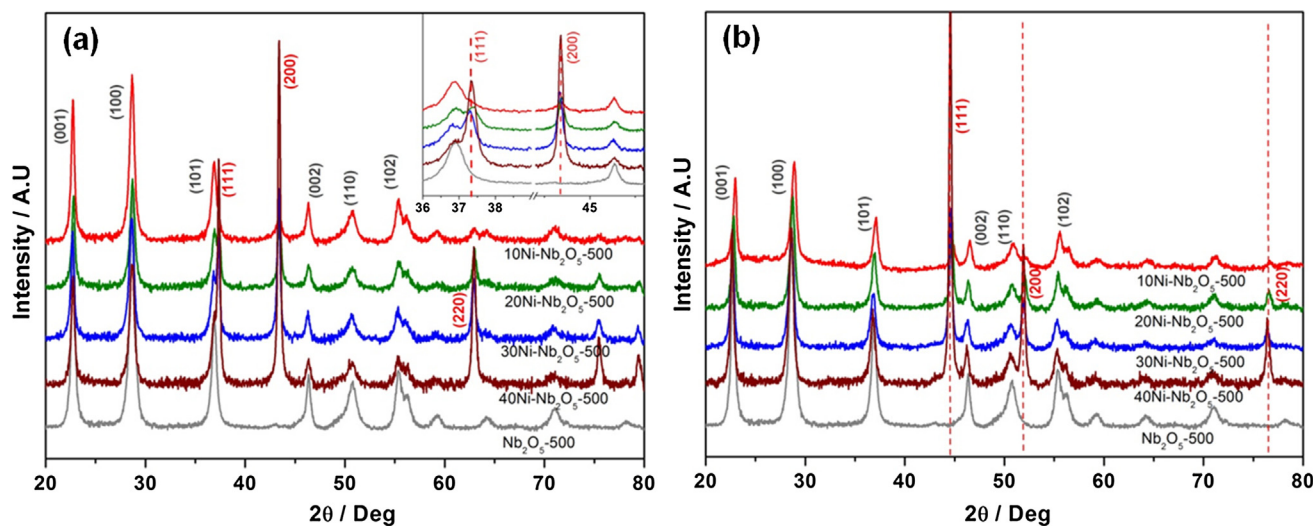


Fig. 2. (a) Powder X-ray diffraction patterns of 10–40 wt% Ni- $\text{Nb}_2\text{O}_5\text{-500}$ catalysts calcined at $400\text{ }^{\circ}\text{C}$ and (b) after CO_2 methanation reaction.

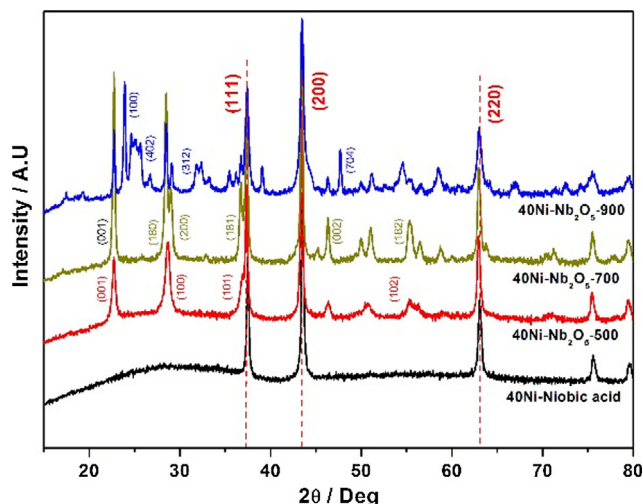


Fig. 3. Powder X-ray diffraction patterns of 40Ni-Nb₂O₅-T catalysts. T indicates the calcination temperature of the support. All catalysts were calcined at 400 °C after nickel impregnation.

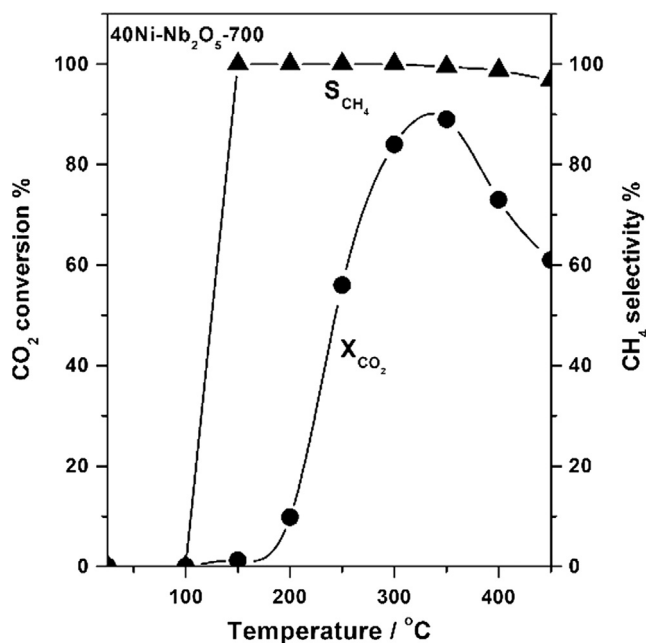


Fig. 4. CO₂ methanation results for 40Ni-Nb₂O₅-700 catalyst with a WHSV of 20,600/h.

(20–40 mesh size) was loaded inside the reactor. The catalysts were reduced in-situ using H₂:N₂ (2:3, v/v) gaseous mixture at 500 °C for 1 h before starting the reaction. Then the reactor temperature was adjusted to the desired reaction temperature. Subsequently, reaction mixture consisting of CO₂ and H₂ in the volumetric ratio of 1:4 was introduced into the reactor with the total flow rate of 12.5 ml/min. For experiments with different space velocity, the gas hourly space velocity (GHSV) was varied between 750/h and 20,600/h by changing the total flow rate of gas while keeping the catalyst mass constant. The outlet of the reactor was analyzed online using an Interscience Compact GC containing Porabond Q column and 5 Å molecular sieve column and two TCD detectors.

3. Results and discussion

CO₂ methanation reaction for all catalysts were carried out in the fixed bed reactor from 23 °C to 450 °C (Fig. 1a). Below 150 °C,

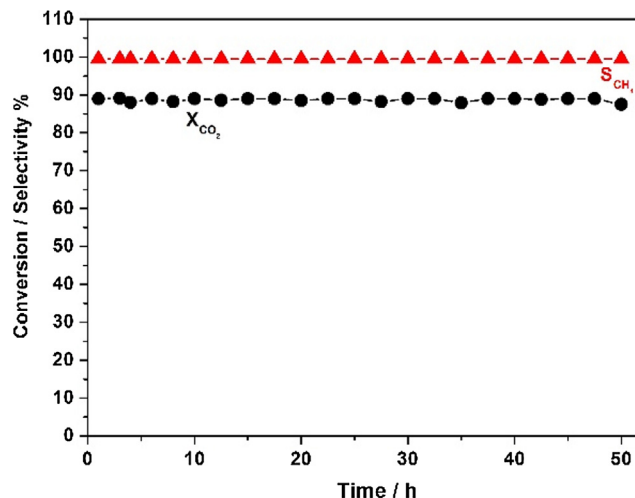


Fig. 5. CO₂ methanation time on stream studies using 40Ni-Nb₂O₅-700 catalyst. 1 g of catalyst was loaded in the fixed bed reactor and total of 50 ml/min gas flow (1:4 volumetric ratio of CO₂:H₂) was used in the methanation reaction.

no CO₂ conversion was observed. With increasing the temperature, CO₂ conversion increased and reached a maximum at 350 °C. Among all catalysts, 40Ni-Nb₂O₅-500 catalysts showed highest conversion (81%) at 325 °C. When higher Ni loading was used, CO₂ conversion was still good, though lower than that of 40Ni-Nb₂O₅-500 catalyst. All catalysts showed more than 99% selectivity towards CH₄ at maximum CO₂ conversion. At temperatures > 350 °C, CO formation is favored and the CO₂ conversion is decreased due to reverse water-gas shift reaction. Pure Nb₂O₅ did not give any CO₂ conversion at 350 °C; thus nickel is necessary to catalyse the reaction. Since 40Ni-Nb₂O₅-500 catalyst was most active, we chose this catalyst for further studies.

Powder XRD patterns of Ni-Nb₂O₅ catalysts are shown in Fig. 2a. Nb₂O₅ can exist in different polymorphic forms upon the heat treatment (Nair et al., 2012). After the calcination at 500 °C, Nb₂O₅ shows strong diffraction peaks at 2θ values of 22.6°, 28.7°, 36.9°, 46.3°, 50.8° and 55.4° which can be indexed as (0 0 1), (1 0 0), (1 0 1), (0 0 2), (1 1 0) and (1 0 2) respectively (JCPDS No. 28-0317) of Nb₂O₅ pseudo hexagonal phase. After loading nickel on Nb₂O₅, new peaks were observed (inset Fig. 1) at 2θ values of 37.2°, 43.4° and 62.9°, which can be assigned to (1 1 1), (2 0 0) and (2 2 0) respectively (JCPDS No. 47-1049) of face centered cubic NiO.

We also characterized the catalysts after the CO₂ hydrogenation reaction by powder XRD (Fig. 2b). The diffraction pattern for the spent catalyst shows that the pseudo hexagonal structure of Nb₂O₅ remains unaltered. However, peaks corresponding to NiO were vanished and new diffraction patterns were observed at 2θ values of 44.5° (1 1 1), 51.9° (2 0 0) and 76.3° (2 2 0). This indicates that NiO is converted to metallic Ni with face centered cubic structure (JCPDS No. 04-0850) after the reaction.

Nb₂O₅ is known for its variable acidic properties and phase transformation when it is heated. To check the influence of thermal treatment of the support on CO₂ methanation, we calcined the niobic acid at different temperatures (500 °C, 700 °C and 900 °C) and then impregnated nickel (40%) on these supports. The CO₂ methanation results are shown in Fig. 1b. For a better comparison, we plotted T₅₀ (temperature at which 50% CO₂ conversion was obtained) in this figure. The catalyst prepared using the support calcined at 700 °C i.e., 40Ni-Nb₂O₅-700 showed maximum CO₂ conversion (92% at around 350 °C). Highest T₅₀ was obtained for 40Ni-Niobic acid (282 °C). The T₅₀ follows the order, 40Ni-Nb₂O₅-700 < 40Ni-Nb₂O₅-900 < 40Ni-Nb₂O₅-500 < 40Ni-Niobic acid.

Table 1
Physico-chemical properties of 40Ni-Nb₂O₅-T[†] catalysts.

| Catalyst | Pretreatment temperature of Nb ₂ O ₅ | BET surface area (m ² /g) | NiO crystallite size (nm) ^{**} | Nb ₂ O ₅ crystallite size (nm) ^{**} | Ni/Nb atomic ratio | T ₅₀ CO ₂ conversion (°C) |
|--|--|--------------------------------------|---|--|--------------------|---|
| 40Ni-Niobic acid | – | 57 | 30 | – | 1.50 | 282 |
| 40Ni-Nb ₂ O ₅ -500 | 500 °C | 57 | 30 | 18 | 1.89 | 274 |
| 40Ni-Nb ₂ O ₅ -700 | 700 °C | 11 | 32 | 32.5 | 3.93 | 242 |
| 40Ni-Nb ₂ O ₅ -900 | 900 °C | 16 | 26 | 38 | 12.7 | 261 |

[†] T = calcination temperature.

^{**} Calculated using Scherrer's equation with the most intense peak.

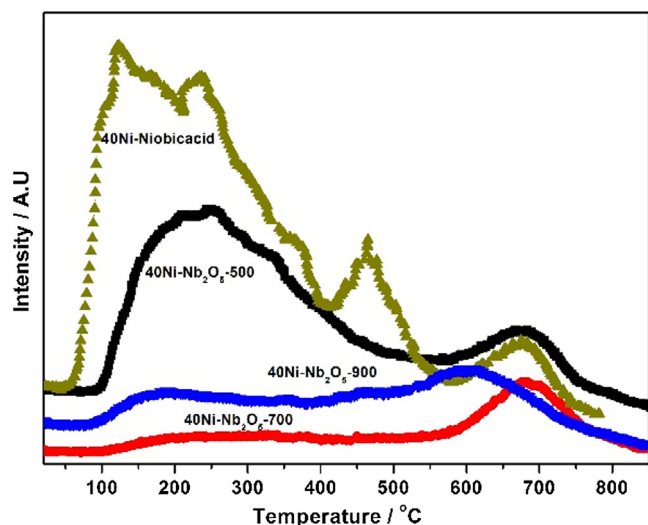


Fig. 6. The ammonia TPD of 40Ni-Nb₂O₅-T catalysts. The pre-treatment temperature of the support has a strong influence on the concentration and strength of the acid sites.

When Nb₂O₅ is subjected to high temperature treatment, three changes can be expected, i.e., change in crystal structure, change in

acidity and change in the surface area. Fig. 3 shows the XRD patterns of 40Ni-Nb₂O₅ catalyst calcined at different temperatures. Without calcination, no strong diffraction peaks of the support are obtained, showing the amorphous nature of the support. Hence, 40Ni-Niobic acid catalyst showed only the diffractions corresponding to fcc NiO. 40Ni-Nb₂O₅-500 catalyst showed diffraction pattern of the pseudo hexagonal phase of Nb₂O₅ as explained above. For 40Ni-Nb₂O₅-700 catalyst, diffraction peaks at 2θ values of 22.6° (0 0 1), 28.4° (1 8 0), 28.9° (2 0 0), 36.7° (1 8 1), 46.2° (0 0 2) and 55.2° (1 8 2) (JCPDS No. 30-0873) are obtained. This shows that Nb₂O₅ has an orthorhombic structure. 40Ni-Nb₂O₅-900 catalyst showed additional peaks at 2θ values of 23.9° (1 0 0), 25.7° (4 0 2) and 47.1° (7 0 4), corresponding to monoclinic phase of Nb₂O₅ (JCPDS No. 37-1468). Thus, 40Ni-Nb₂O₅-900 contains a mixture of orthorhombic and monoclinic phases. Irrespective of the different polymorphs of Nb₂O₅, all catalysts showed diffraction peaks of face centered cubic NiO.

To check the efficiency of the 40Ni-Nb₂O₅-700 catalyst at higher flow rates of the feed, we carried out CO₂ methanation at a WHSV of 20,600/h. As shown in Fig. 4, the CO₂ conversion kinetics was similar. Maximum CO₂ conversion (89%) was obtained at 350 °C which is almost same as the CO₂ conversion at a WHSV of 750/h. Selectivity towards CH₄ was more than 99% at 350 °C. We also did time on stream studies for 50 h using 40Ni-Nb₂O₅-700 catalyst (Fig. 5). The CO₂ conversion and selectivity for CH₄ were unaltered. This shows that the catalyst is highly resistant to coke formation. Thermogravimetry measurement (not shown), showed only small

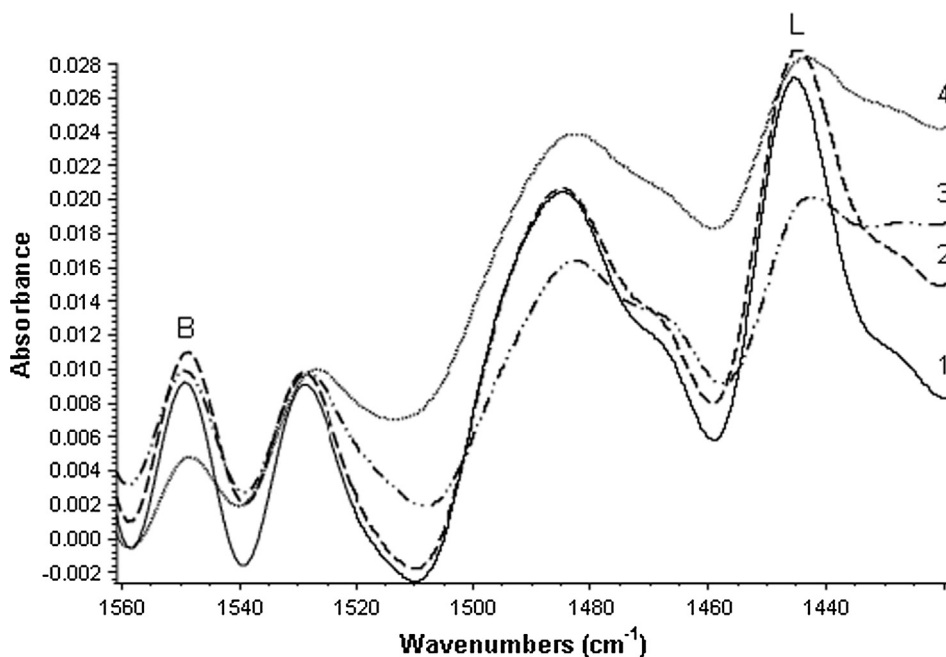


Fig. 7. DRIFT spectra of pyridine adsorbed on 40Ni-Nb₂O₅-T catalysts. (1) 40Ni-Niobic acid (2) 40Ni-Nb₂O₅-500 (3) 40Ni-Nb₂O₅-700 and (4) 40Ni-Nb₂O₅-900.

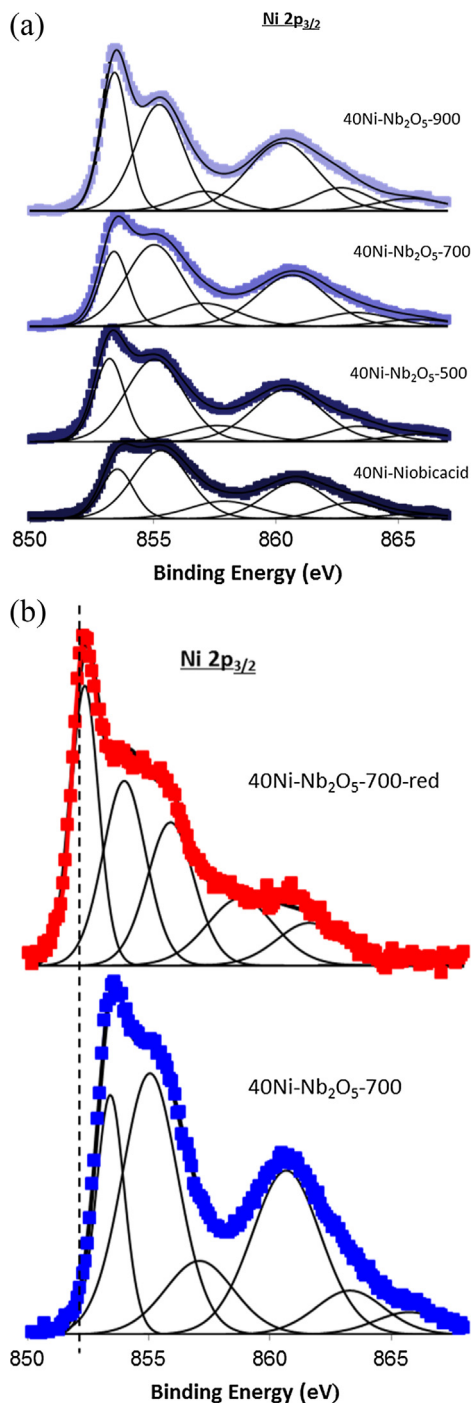


Fig. 8. Ni $2p_{3/2}$ XPS of 40Ni-Nb₂O₅-T catalysts. In (a) the pre-treatment temperature of the niobia support is different and in (b) the fresh and spent samples of 40Ni-Nb₂O₅-700 are compared.

amount of coke on the catalyst after 50 h of reaction. Please note that we only report a simple analysis here; however, thermogravimetric study can be more complicated. The oxidation of Ni to NiO can lead to a weight gain, which could interfere with the weight loss due to coke removal. The diffusion of coke into the subsurface/bulk was observed for Pd in previous studies and it cannot be ruled out for Ni without further detailed studies; however, this is out of the scope of this paper.

We characterized the catalysts with various techniques to correlate the catalytic activity with the catalyst structure. Table 1

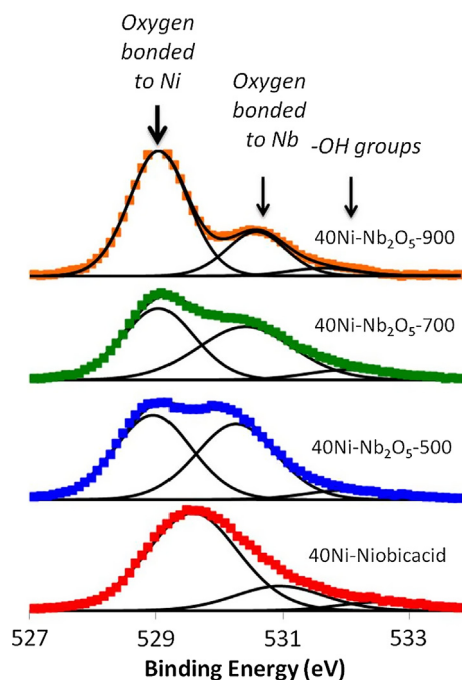


Fig. 9. O 1s XPS of 40Ni-Nb₂O₅-T catalysts. The spectra can be deconvoluted into three indicating the presence of three types of oxygen species.

shows the BET surface areas of the catalysts. 40Ni-Niobic acid and 40Ni-Nb₂O₅-500 catalysts have same surface area of 57 m²/g. As the pre-treatment temperature of niobia increased, the surface area started to decrease. 40Ni-Nb₂O₅-700 and 40Ni-Nb₂O₅-900 catalysts had similar surface areas, which are much lower than the catalysts calcined at lower temperature, as expected. Despite having low surface area, 40Ni-Nb₂O₅-700 catalyst showed the best activity, indicating that the surface area has no direct correlation with activity in this case. The crystallite sizes of the calcined catalysts were calculated by the Scherrer equation using the most intense diffraction peaks of nickel and niobia. Table 1 shows these values. Niobic acid was amorphous; so no value is reported for this. For samples calcined at higher temperatures, the crystallite size increased with increasing calcination temperature, indicating higher crystallinity. Since the calcination was done at the same temperature after loading nickel, the crystallite size of nickel does not vary significantly. Please note that the absolute values may not be accurate, since several factors can influence the peak width in XRD. Instead, we can use these numbers as an indication of the trend in crystallite sizes. The values show that there is no significant difference in crystallite sizes of Ni when it is loaded on niobia calcined at temperatures of 500 °C or 700 °C or uncalcined. Thus, the crystallite size is not a major factor in determining the catalytic activity. However, when Ni is loaded on niobia calcined at 900 °C, a smaller crystallite size is observed. The Ni/Nb atomic ratio obtained from XPS increased with the calcination temperature of niobia indicating that there is a surface enrichment of nickel. Though 40Ni-Nb₂O₅-900 shows the highest surface enrichment of Ni, it is not the most active catalyst which prevents a direct correlation of surface Ni content with the activity. A direct correlation with a single catalyst characteristic seems to be not possible; thus, the activity may be determined by a combination of characteristics.

The acidity of the catalyst can be significantly affected by the temperature of the heat treatment. Hence, strength of the acid sites in 40 wt%Ni loaded niobia catalysts were analyzed by temperature programmed desorption of ammonia between 30 °C and 900 °C

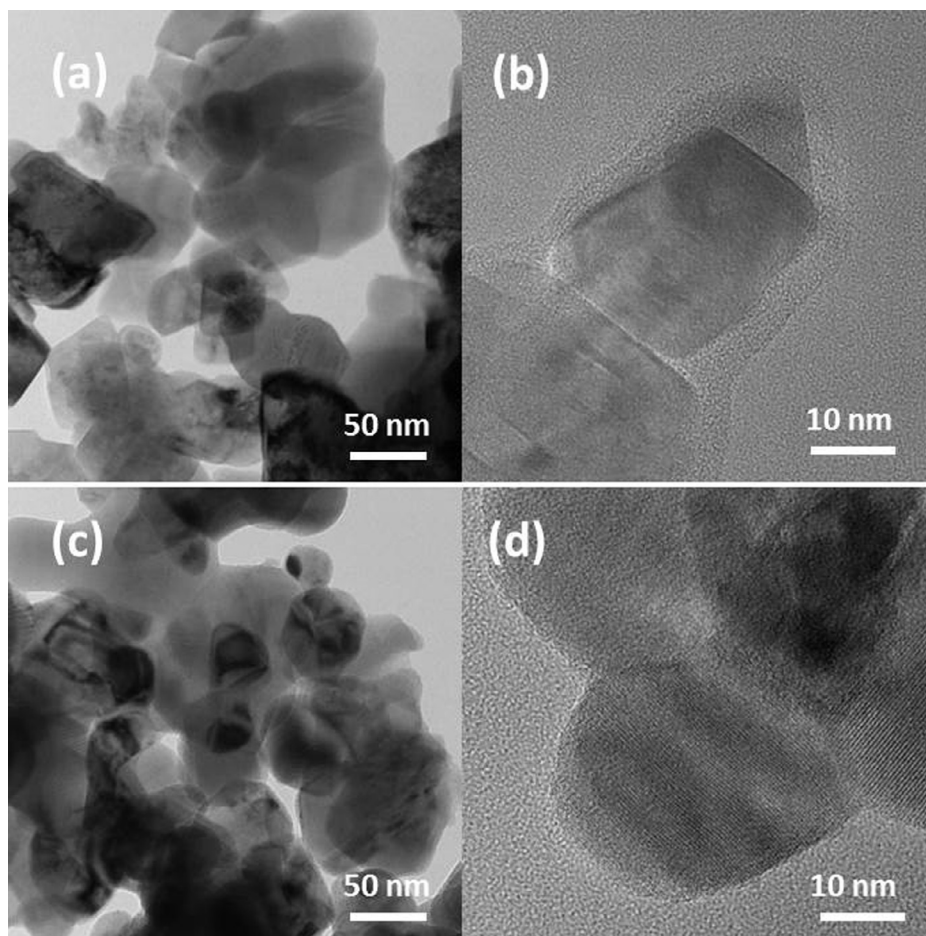


Fig. 10. TEM images of fresh [(a) and (b)] and spent [(c) and (d)] 40Ni-Nb₂O₅-700 catalysts.

(Fig. 6). The NH₃-TPD profiles of 40Ni-Nb₂O₅-T catalysts showed a low temperature desorption peak, which can be assigned to the interaction of NH₃ molecules with weak acid sites. The peak at 500 °C observed for 40Ni-Niobic acid catalyst could be due to the dehydroxylation of the surface OH groups of niobic acid (Marakatti et al., 2016). NH₃ desorption peak observed around 700 °C can be assigned to the presence of strong acidic sites in the catalysts. Total acidic sites are decreased as the niobia pre-treatment temperature increases. This is due to the decrease in the surface area of the catalysts and dehydroxylation of surface hydroxyl groups at high temperature. 40Ni-Nb₂O₅-700 and 40Ni-Nb₂O₅-900 catalysts contain higher concentration of strong acidic sites than weak acidic sites. In 40Ni-Nb₂O₅-700 catalyst, desorption of NH₃ from strong acid sites occurred at higher temperature (maximum desorption around 700 °C) compared with 40Ni-Nb₂O₅-900 catalyst (630 °C). To study the contribution from Brønsted and Lewis acidities, we did the DRIFT-IR study of pyridine adsorbed on 40Ni-Nb₂O₅-T catalysts (Fig. 7). The DRIFT spectra obtained are of rather low quality for a quantitative analysis, probably because of the high Ni loading (40%). However, qualitatively, we can infer that the Lewis acidity (L) dominates in these samples. The density of acid sites, both Lewis (L) and Brønsted (B), decreases with the temperature of pretreatment, with the B/L ratio practically unchanged (B/L = 0.28–0.32). Both techniques confirm that high temperature treated catalyst contains more Lewis acid sites. The catalysts with strong acid sites are also better in terms of catalytic performance; however, it is difficult to assign a reason for this.

Ni 2p_{3/2} XPS of 40Ni-Nb₂O₅-T samples are shown in Fig. 8a. 40Ni-Niobic acid catalyst shows a multiplet split at 853.9, 855.7 and 858.4 eV. These peaks are characteristic of Ni²⁺ species. Absence of a peak at 852.7 eV confirms there is no metallic Ni species in this sample. As the pre-treatment temperature of Nb₂O₅ changes, there is a change in the peak ratio of the multiplet. Since the multiplets are usually ascribed to the interference in the electron core levels, the change observed here shows that the electron density of nickel center varies. This could be due to an interaction between the support and NiO. This also indicates that there is a stronger metal-support interaction when the support is pre-treated at higher temperatures.

Similar trends were not clearly seen in the XPS of Nb core level. It is because the Nb has less electrons in the d level and changes are more difficult to be observed. Fig. 8b shows the comparison of Ni 2p_{3/2} peaks of fresh and spent 40Ni-Nb₂O₅-700 catalysts. Ni 2p_{3/2} multiplet of spent catalyst (852.1 eV) is observed at lower BE than the fresh catalyst (852.9). This shows that the Ni is in a reduced state during the reaction. Ni/Nb atomic ratios in different catalysts are shown in Table 1. As pre-treatment temperature increases, the amount of Ni on the surface is higher. 40Ni-Nb₂O₅-900 catalyst contains highest Ni/Nb surface ratio of 12.7. 40Ni-Nb₂O₅-700 catalyst, which is the most active, has Ni/Nb ratio of 3.93. Other two catalysts have lower Ni/Nb ratios. O 1s spectra of 40Ni-Nb₂O₅-T catalysts are shown in Fig. 9. They can be deconvoluted into three different peaks corresponding to surface hydroxyl groups, oxygen bonded to Nb and oxygen bonded to Ni. The changes in the O 1s B.E. can be caused by different covalence degrees of the metal-

oxygen bond, resulting in changes in the negative charge and basicity of the oxygen. 40Ni-Nb₂O₅-900 catalyst has more oxygen bonded with Ni compared to other catalysts.

TEM images of fresh and spent (after 50 h of reaction) 40Ni-Nb₂O₅-700 catalysts are shown in Fig. 10. NiO particles are (Fig. 10(a) and (b)) present as rectangular slabs on Nb₂O₅. Fig. 10(c) and (d) show the images of spent 40Ni-Nb₂O₅-700 catalyst. There is no major agglomeration of Ni particles in spent 40Ni-Nb₂O₅-700 catalyst, indicating that the catalyst is stable during the reaction, in agreement with the long-term reaction study (Fig. 5). Ni-agglomeration tends to happen however, and may increase with further time on stream.

4. Conclusions

In this work, we prepared highly active and selective CO₂ methanation catalysts based on nickel and niobia. At atmospheric pressure and 350 °C, the catalyst 40Ni-Nb₂O₅-700 gave CO₂ conversion of 92% and CH₄ selectivity of 99%. The results show that the pre-treatment temperature of the niobia support is important in determining the final catalyst performance. The catalyst showed stable activity during a continuous test of 50 h. The pre-treatment temperature affects the density and strength of the acid sites on the final catalyst. Strong acid sites seems to be more favourable for the CO₂ hydrogenation, though we couldn't assign a direct reason for this.

Acknowledgment

E.S.G. and N.R.S acknowledge the financial support from NWO CAPITA project (732.013.002). ASE acknowledges the financial support from the MINECO projects MAT-2013-45008-P and MAT2016-81732-ERC. EVRF gratefully acknowledge support from MINECO for his Ramón y Cajal grant (RyC-2012-11427) and University of Alicante for the project GRE-13-31. Generalitat Valenciana is also acknowledged for financial support (PROMETEOII/ 2014/004).

References

- Aziz, M.A.A., Jalil, A.A., Triwahyono, S., Ahmad, A., 2015. CO₂ methanation over heterogeneous catalysts: recent progress and future prospects. *Green Chem.* 17, 2647–2663.
- Bajpai, P.K., Bakhshi, N.N., Mathews, J.F., 1982. Deactivation studies of nickel catalysts used in the methanation of carbon monoxide. *Can. J. Chem. Eng.* 60, 4–10.
- Barrientos, J., Lualdi, M., Boutonnet, M., Jaras, S., 2014. Deactivation of supported nickel catalysts during CO methanation. *Appl. Catal. A-Gen.* 486, 143–149.
- Batyrev, E.D., Shiju, N.R., Rothenberg, G., 2012. Exploring the Activated state of Cu/ZnO(0001)-Zn, a model catalyst for methanol synthesis. *J. Phys. Chem. C* 116, 19335–19341.
- Cai, W., Zhong, Q., Zhao, Y.X., 2013. Fractional-hydrolysis-driven formation of non-uniform dopant concentration catalyst nanoparticles of Ni/Ce_xZr_{1-x}O₂ and its catalysis in methanation of CO₂. *Catal. Commun.* 39, 30–34.
- Chary, K.V.R., Lakshmi, K.S., Rao, P.V.R., Rao, K.S.R., Papadaki, M., 2004. Characterization and catalytic properties of niobia supported nickel catalysts in the hydrodechlorination of 1,2,4-trichlorobenzene. *J. Mol. Catal. A-Chem.* 223, 353–361.
- Crowley, T.J., 2000. Causes of climate change over the past 1000 years. *Science* 289, 270–277.
- Davis, S.J., Caldeira, K., Matthews, H.D., 2010. Future CO₂ emissions and climate change from existing energy infrastructure. *Science* 329, 1330–1333.
- Daza, Y.A., Kuhn, J.N., 2016. CO₂ conversion by reverse water gas shift catalysis: comparison of catalysts, mechanisms and their consequences for CO₂ conversion to liquid fuels. *RSC Adv.* 6, 49675–49691.
- den Otter, J., de Jong, K.P., 2014. Highly selective and active niobia-supported cobalt catalysts for Fischer-Tropsch synthesis. *Top. Catal.* 57, 445–450.
- den Otter, J.H., Yoshida, H., Ledesma, C., Chen, D., de Jong, K.P., 2016. On the superior activity and selectivity of PtCo/Nb₂O₅ Fischer-Tropsch catalysts. *J. Catal.* 340, 270–275.
- Friedlingstein, P., Houghton, R., Marland, G., Hackler, J., Boden, T.A., Conway, T., Canadell, J., Raupach, M., Riais, P., Le Quere, C., 2010. Update on CO₂ emissions. *Nature Geosci.* 3, 811–812.
- Frontera, P., Macario, A., Ferraro, M., Antonucci, P., 2017. Supported catalysts for CO₂ methanation: a review. *Catalysts* 7, 59.
- Frydman, A., Castner, D.G., Campbell, C.T., Schmal, M., 1999. Carbon monoxide hydrogenation on Co-Rh/Nb₂O₅ catalysts. *J. Catal.* 188, 1–13.
- Gao, J., Wang, Y., Ping, Y., Hu, D., Xu, G., Gu, F., Su, F., 2012. A thermodynamic analysis of methanation reactions of carbon oxides for the production of synthetic natural gas. *RSC Adv.* 2, 2358–2368.
- Götz, M., Lefebvre, J., Mörsa, F., Koch, A.M., Graf, F., Bajohr, S., Reimert, R., Kolb, T., 2016. Renewable power-to-gas: a technological and economic review. *Renew. Energy* 85, 1371–1390.
- Inui, T., Takeguchi, T., 1991. Effective conversion of carbon dioxide and hydrogen to hydrocarbons. *Catal. Today* 10, 95–106.
- Jardim, E.D., Rico-Frances, S., Abdelouhab-Reddam, Z., Coloma, F., Silvestre-Albero, J., Sepulveda-Escribano, A., Ramos-Fernandez, E.V., 2015. High performance of Cu/CeO₂-Nb₂O₅ catalysts for preferential CO oxidation and total combustion of toluene. *Appl. Catal. A-Gen.* 502, 129–137.
- Junaedi, C., Hawley, K., Walsh, D., Roychoudhury, S., Abney, M., Perry, J., 2011. Compact and lightweight Sabatier reactor for carbon dioxide reduction. 41st International Conference on Environmental Systems. Portland, Oregon.
- Khorsand, K., Marvast, M.A., Pooladian, N., Kakavand, M., 2007. Modeling and simulation of methanation catalytic reactor in ammonia unit. *Petrol. Coal* 49, 46–53.
- Lu, H.L., Yang, X.Z., Gao, G.J., Wang, K.B., Shi, Q.Q., Wang, J., Han, C.H., Liu, J., Tong, M., Liang, X.Y., Li, C.F., 2014. Mesoporous zirconia-modified clays supported nickel catalysts for CO and CO₂ methanation. *Int. J. Hydrogen Energy* 39, 18894–18907.
- Marakatti, V.S., Manjunathan, P., Halgeri, A.B., Shanbhag, G.V., 2016. *Catal. Sci. Technol.* 6, 2268–2279.
- Meehl, G.A.W.M., Washington, W.D., Collins, J.M., Arblaster, A.X., Hu, B., Buja, L.E., Strand, W.G., Teng, H.Y., 2005. How much more global warming and sea level rise? *Science* 307, 1769–1772.
- Mejia, C.H., Raja, E.S., Olivos-Suarez, A., Gascon, J., Greer, H.F., Zhou, W., Rothenberg, G., Shiju, N.R., 2016. Ru/TiO₂-catalysed hydrogenation of xylose: the role of crystal structure of the support. *Catal. Sci. Technol.* 6, 577–582.
- Mozer, T.S., Passos, F.B., 2011. Selective CO oxidation on Cu promoted Pt/Al₂O₃ and Pt/Nb₂O₅ catalysts. *Int. J. Hydrogen Energy* 36, 13369–13378.
- Nair, G.S., Adrijanto, E., Alsalmeh, A., Kozhevnikov, I.V., Cooke, D.J., Brown, D.R., Shiju, N.R., 2012. Glycerol utilization: solvent-free acetalisation over niobia catalyst. *Catal. Sci. Technol.* 2, 1173–1179.
- Nie, W., Zou, X., Chen, C., Wang, X., Ding, W., Lu, X., 2017. Methanation of carbon dioxide over Ni-Ce-Zr oxides prepared by one-pot hydrolysis of metal nitrates with ammonium carbonate. *Catalysts* 7, 104.
- Nowak, I., Ziolek, M., 1999. Niobium compounds: preparation, characterization, and application in heterogeneous catalysis. *Chem. Rev.* 99, 3603–3624.
- Polanski, J., Siudyga, T., Bartczak, P., Kapkowski, M., Ambrozkiwicz, W., Nobis, A., Sitko, R., Klimontko, J., Szade, J., Lelątko, J., 2017. Oxide passivated Ni-supported Ru nanoparticles in silica: a new catalyst for low-temperature carbon dioxide methanation. *Appl. Catal. B: Environ.* 206, 16–23.
- Porosoff, M.D., Yan, B., Chen, J.G., 2016. Catalytic reduction of CO₂ by H₂ for synthesis of CO, methanol and hydrocarbons: challenges and opportunities. *Energy Environ. Sci.* 9, 62–73.
- Rockström, J., Gaffney, O., Rogelj, J., Meinshausen, M., Nakicenovic, N., Schellnhuber, H.J., 2017. A roadmap for rapid decarbonization. *Science* 355, 1269–1271.
- Rojas, E., Guerrero-Perez, M.O., Banares, M.A., 2009. Direct ammoxidation of ethane: an approach to tackle the worldwide shortage of acetonitrile. *Catal. Commun.* 10, 1555–1557.
- Saeidi, S., Amin, N.A.S., Rahimpour, M.R., 2014. Hydrogenation of CO₂ to value-added products—a review and potential future developments. *J. CO₂ Utiliz.* 5, 66–81.
- Shiju, N.R., Brown, D.R., Wilson, K., Rothenberg, G., 2010. Glycerol valorization: dehydration to acrolein over silica-supported niobia catalysts. *Top. Catal.* 53, 1217–1223.
- Tada, S., Shimizu, T., Kameyama, H., Haneda, T., Kikuchi, R., 2012. Ni/CeO₂ catalysts with high CO₂ methanation activity and high CH₄ selectivity at low temperatures. *Int. J. Hydrogen Energy* 37, 5527–5531.
- Wachs, I.E., 2005. Recent conceptual advances in the catalysis science of mixed metal oxide catalytic materials. *Catal. Today* 100, 79–94.
- Wang, W., Wang, S., Ma, X., Gong, J., 2011. Recent advances in catalytic hydrogenation of carbon dioxide. *Chem. Soc. Rev.* 40, 3703–3727.
- Wei, W., Jinlong, G., 2011. Methanation of carbon dioxide: an overview. *Front. Chem. Sci. Eng.* 5, 2–10.
- Wojcieszak, R., Jasik, A., Monteverdi, S., Ziolek, M., Bettahar, M.M., 2006. Nickel niobia interaction in non-classical Ni/Nb₂O₅ catalysts. *J. Mol. Catal. A-Chem.* 256, 225–233.
- Yang, H., Xu, Z., Fan, M., Gupta, R., Slimane, R.B., Bland, A.E., Wright, I., 2008. Progress in carbon dioxide separation and capture: a review. *J. Environ. Sci.* 20, 14–27.
- Yu, K.M.K., Curcic, I., Gabriel, J., Tsang, S.C.E., 2008. Recent advances in CO₂ capture and utilization. *ChemSusChem* 1, 893–899.
- Zhang, X., Bauer, C., Mutel, C.L., Volkart, K., 2017. Life cycle assessment of power-to-gas: approaches, system variations and their environmental implications. *Appl. Energy* 190, 326–338.
- Zhou, L., Wang, Q., Ma, L., Chen, J., Ma, J., Zi, Z., 2015. CeO₂ promoted Mesoporous Ni/γ-Al₂O₃ catalyst and its reaction conditions for CO₂ methanation. *Catal. Lett.* 145, 612–619.